

A Globally Convergent Gauss-Newton Algorithm for AC Optimal Power Flow

Ilyes Mezghani, Quoc Tran-Dinh, Ion Necoara, Anthony Papavasiliou

Abstract—We propose a globally convergent and robust Gauss-Newton algorithm for finding a (local) optimal solution of a non-convex and possibly non-smooth optimization problem arising from AC optimal power flow on meshed networks. The algorithm that we present is based on a Gauss-Newton-type iteration for an exact penalty reformulation of the power flow problem. We establish a global convergence rate for such a scheme from any initial point to a stationary point of the problem while using an exact penalty formulation to gain numerical robustness against ill-conditioning. We compare our algorithm with a well-established solver, IPOPT, on several representative problem instances in MATPOWER. We demonstrate the comparable, but more robust, performance of our method for a variety of the MATPOWER test cases.

Index Terms—AC optimal power flow, non-convex optimization, penalty reformulation, Gauss-Newton method.

I. INTRODUCTION

The optimal power flow (OPF) problem [1] consists in finding an optimal operating point of a power system while minimizing a certain objective (typically power generation cost), subject to the Kirchhoff's power flow equations and various network and control operating limits. We focus in this paper on the alternating current optimal power flow (AC-OPF) problem [2], which lies at the heart of short-term power system operations [3]. The increasing integration of distributed resources that are connected to medium and low-voltage networks has increased the relevance of AC-OPF as an appropriate framework of modeling operational constraints that affect the coordination of transmission and distribution system operations [4].

a) *Related work*: In recent years, there has been a great body of literature that has focused on convex relaxations of the AC-OPF problem, including semidefinite programming relaxations [5], [6], conic relaxations [7], [8], [9], and quadratic relaxations [10]. These works have established conditions under which these relaxations are exact, and understanding cases in which this is not so [11]. Instead, our interest in the present paper is to tackle directly this problem as a non-convex optimization problem with non-linear equality constraints. Such a formulation is sufficiently general to produce physically implementable solutions in the context of realistic system operations.

Our interest in this application is driven by recent research on the integration of transmission and distribution system operations [12] in the context of the SmartNet EU project [13]. The standard linear approximations of power flow are inadequate for medium and low-voltage distribution networks, where real power losses are significant, reactive power flows are non-negligible, and voltage constraints are relevant. Moreover, the

complexity of the network (meshed transmission networks and almost-radial distribution networks [14]) renders the existing relaxations inexact, and the resulting dispatch possibly non-implementable. This necessitates empirical operator interventions, and undermines our ability to actively engage large numbers of distributed resources in short-term power system operations.

The AC-OPF problem is usually formulated as a non-convex optimization problem. It is well-known that optimization problems with non-convex constraints are difficult to solve. Classical techniques such as interior-point, augmented Lagrangian, penalty, Gauss-Newton, and sequential quadratic programming methods can only aim at finding a stationary point, which is a candidate for a local minimum [15], [16]. For an iterative method to identify a stationary point that is a local minimum, but not a saddle-point, more sophisticated techniques are required, such as cubic regularization [17] or random noise gradient [18]. However, these methods are often very difficult to implement and inefficient in large-scale problems with non-convex constraints. One of the most efficient and well-established nonlinear solvers for finding stationary points is IPOPT [19], which relies on a primal-dual interior-point method combined with other advanced techniques. We emphasize that this classical method is only guaranteed to converge to a stationary point, and often requires a strategy such as line-search, filter, or trust-region to achieve global convergence under certain restrictive assumptions. Moreover, each iteration of IPOPT requires solving a non-convex subproblem via linearization combined with a line-search or filter strategy.

b) *Our approach and contributions*: In this paper, we consider an AC optimal power flow problem over large-scale networks. We are interested in an approach that can tackle general meshed networks. We show that this problem can be posed in the framework of non-convex optimization with a particular structure on the constraints. Based on this structure we devise a provable convergent Gauss-Newton (GN)-type algorithm for solving this non-convex problem. Our algorithm converges globally to a stationary point of the problem from any starting point. In addition, it is also different from standard GN methods in the literature due to the use of a non-smooth penalty instead of a classical quadratic penalty term. This allows our algorithm to converge globally and also to be more robust to ill-conditioning [20]. Hence, we refer to this algorithm as a *global and robust* GN scheme. The main idea of our method is to keep the convex sub-structure of the original problem unchanged and to convexify the non-convex part by exploiting penalty theory and the GN framework. Hence, in contrast to IPOPT, each iteration of our algorithm requires

solving a convex subproblem, which can efficiently be solved by many existing convex solvers such as CPLEX or Gurobi.

The main contributions of the paper are the following:

- (i) We consider a quadratic reformulation of the AC-OPF problem, as in [7], [21], and propose an exact penalty reformulation of the problem in order to handle the non-convex equality constraints and a novel global and robust GN algorithm for solving the corresponding problem.
- (ii) For our optimization algorithm, we prove that its iterate sequence converges globally (i.e. from any starting point) to a stationary point of the underlying problem. We also estimate its best-known global sublinear convergence rate.
- (iii) We show that the newly developed algorithm can be implemented efficiently on AC-OPF problems and test it on several numerical examples from the well-known MATPOWER test cases [22], [23]. We observe competitive, and often superior and more robust, performance to the well-established and widely-used IPOPT solver.

Our algorithm is simple to implement and can be incorporated flexibly with any available convex sub-solver that supports a warm start strategy in order to gain efficiency.

c) Content: The paper is organized as follows. In Section II, we present the AC-OPF problem and its quadratic reformulation. In Section III, we introduce our Gauss-Newton algorithm and analyze its convergence properties. Finally, in Section IV, we adapt the algorithm to the AC-OPF problem and test it on several representative MATPOWER test cases.

II. MATHEMATICAL MODELING

A. Problem settings

Consider a directed power network with a set of nodes \mathcal{B} and a set of branches \mathcal{L} . The network consists of a set \mathcal{G} of generators, with \mathcal{G}_i denoting the set of generators at bus i . Denote $Y = G + jB$ as the system admittance matrix.

The decision variables of AC-OPF are the voltage magnitudes $\mathbf{v} \in \mathbb{R}^{|\mathcal{B}|}$, phase angles $\boldsymbol{\theta} \in \mathbb{R}^{|\mathcal{B}|}$, and the real and reactive power outputs of generators, which are denoted as $\mathbf{p} \in \mathbb{R}^{|\mathcal{G}|}$ and $\mathbf{q} \in \mathbb{R}^{|\mathcal{G}|}$. We will consider a fixed real and reactive power demand at every node i , which we denote as P_i^d and Q_i^d , respectively.

The constraints of the AC-OPF problem can be described by equations (1)-(5), see [9]. Constraints (1) and (2) correspond to the real and reactive power balance equations of node i . Constraints (3) and (4) impose complex power flow limits on each line, which we indicate by a parameter matrix \mathbf{S} . Constraints (5) impose bounds on voltage magnitudes (indicated by parameter vectors $\underline{\mathbf{V}}$ and $\overline{\mathbf{V}}$), bounds on real power magnitudes (indicated by parameter vectors $\underline{\mathbf{P}}$ and $\overline{\mathbf{P}}$), bounds on reactive power magnitudes (indicated by parameter vectors $\underline{\mathbf{Q}}$ and $\overline{\mathbf{Q}}$), and bounds on voltage phase angles (indicated by parameter vectors $\underline{\boldsymbol{\theta}}$ and $\overline{\boldsymbol{\theta}}$). Note that the power balance equality constraints (1), (2) as well as the inequality constraints (3), (4) are non-convex with respect to \mathbf{v} and $\boldsymbol{\theta}$.

We will consider an objective of minimizing real power generation costs. Hence, we consider a convex quadratic objective function f :

$$f(\mathbf{p}) = \mathbf{p}^\top \text{diag}(\mathbf{C}_2) \mathbf{p} + \mathbf{C}_1^\top \mathbf{p},$$

where $\mathbf{C}_2 \geq 0$ and \mathbf{C}_1 are given coefficients of the cost function.

The AC OPF problem then reads as the following non-convex optimization problem:

$$\mathcal{P}_{opt} : \quad \min_{(\mathbf{v}, \boldsymbol{\theta}, \mathbf{p}, \mathbf{q})} f(\mathbf{p}) \quad \text{subject to (1), (2), (3), (4), (5).}$$

B. Quadratic reformulation

The starting point of our proposed GN method for solving problem \mathcal{P}_{opt} is the quadratic reformulation of AC-OPF [21]. In this reformulation, we use a new set of variables c_{ij} and s_{ij} for replacing the voltage phasors $v_i \angle \theta_i$. These new variables are defined for all $i \in \mathcal{B}$ and $(i, j) \in \mathcal{L}$ as:

$$\begin{aligned} c_{ii} &= v_i^2, & c_{ij} &= v_i v_j \cos(\theta_i - \theta_j), & (6) \\ s_{ii} &= 0, & s_{ij} &= -v_i v_j \sin(\theta_i - \theta_j), & (7) \end{aligned}$$

where we will denote the vectors \mathbf{c} and \mathbf{s} as the collection of the c_{ij} and s_{ij} variables, respectively.

For $\underline{\boldsymbol{\theta}} \leq \boldsymbol{\theta} \leq \overline{\boldsymbol{\theta}}$, the mapping from $(\mathbf{v}, \boldsymbol{\theta})$ to (\mathbf{c}, \mathbf{s}) defined by (6), (7) can be inverted as follows:

$$v_i = \sqrt{c_{ii}}, \quad \theta_i - \theta_j = \arctan\left(-\frac{s_{ij}}{c_{ij}}\right),$$

thereby defining a bijection in (\mathbf{c}, \mathbf{s}) and $(\mathbf{v}, \boldsymbol{\theta})$.

The set of (\mathbf{c}, \mathbf{s}) and $(\mathbf{v}, \boldsymbol{\theta})$ that define this bijection is further *equivalent* to the following set of non-linear non-convex constraints in $(\mathbf{c}, \mathbf{s}, \mathbf{v}, \boldsymbol{\theta})$, see [9]:

$$\begin{aligned} c_{ij}^2 + s_{ij}^2 &= c_{ii} c_{jj} & \forall (i, j) \in \mathcal{L} & (8) \\ \sin(\theta_i - \theta_j) c_{ij} + \cos(\theta_i - \theta_j) s_{ij} &= 0 & \forall (i, j) \in \mathcal{L} & (9) \\ s_{ii} &= 0 & \forall i \in \mathcal{B}. & \end{aligned}$$

Now, we will substitute the voltage magnitude variables into the problem \mathcal{P}_{opt} , and consider the problem on the variables $(\mathbf{c}, \mathbf{s}, \boldsymbol{\theta})$. This reformulation has been commonly employed in the literature in order to arrive at an SOCP relaxation of the problem [21], [7]. Through numerical experiments, we demonstrate that this reformulation results in highly effective starting points for our algorithm based on the SOCP relaxation of the AC-OPF. Moreover, the reformulation preserves the power balance constraints in linear form. Thus, the power balance constraints are not penalized in our scheme, which implies that they are respected at every iteration of the algorithm. For all these reasons, we pursue the quadratic reformulation of the present section, despite the fact that it requires the introduction of the new variables \mathbf{c} and \mathbf{s} .

Concretely, the AC power balance constraints (1) and (2) are linear in c_{ij} and s_{ij} :

$$\begin{aligned} \sum_{j \in \mathcal{G}_i} p_j - P_i^d - G_{ii} c_{ii} - \sum_{(i,j) \in \mathcal{L}} (G_{ij} c_{ij} - B_{ij} s_{ij}) \\ - \sum_{(j,i) \in \mathcal{L}} (G_{ji} c_{ji} - B_{ji} s_{ji}) &= 0 \quad \forall i \in \mathcal{B}, & (10) \\ \sum_{j \in \mathcal{G}_i} q_j - Q_i^d + B_{ii} c_{ii} + \sum_{(i,j) \in \mathcal{L}} (B_{ij} c_{ij} + G_{ij} s_{ij}) \\ + \sum_{(j,i) \in \mathcal{L}} (B_{ji} c_{ji} + G_{ji} s_{ji}) &= 0 \quad \forall i \in \mathcal{B}, & (11) \end{aligned}$$

$$\begin{aligned} & \sum_{j \in \mathcal{G}_i} p_j - P_i^d - G_{ii} v_i^2 - \sum_{(i,j) \in \mathcal{L}} v_i v_j \left(G_{ij} \cos(\theta_i - \theta_j) + B_{ij} \sin(\theta_i - \theta_j) \right) \\ & - \sum_{(j,i) \in \mathcal{L}} v_j v_i \left(G_{ji} \cos(\theta_j - \theta_i) + B_{ji} \sin(\theta_j - \theta_i) \right) = 0 \quad \forall i \in \mathcal{B}, \end{aligned} \quad (1)$$

$$\begin{aligned} & \sum_{j \in \mathcal{G}_i} q_j - Q_i^d + B_{ii} v_i^2 - \sum_{(i,j) \in \mathcal{L}} v_i v_j \left(G_{ij} \sin(\theta_i - \theta_j) - B_{ij} \cos(\theta_i - \theta_j) \right) \\ & - \sum_{(j,i) \in \mathcal{L}} v_j v_i \left(G_{ji} \sin(\theta_j - \theta_i) - B_{ji} \cos(\theta_j - \theta_i) \right) = 0 \quad \forall i \in \mathcal{B}, \end{aligned} \quad (2)$$

$$\begin{aligned} & \left(-G_{ii} v_i^2 + G_{ij} v_i v_j \cos(\theta_i - \theta_j) + B_{ij} v_i v_j \sin(\theta_i - \theta_j) \right)^2 \\ & + \left(B_{ii} v_i^2 - B_{ij} v_i v_j \cos(\theta_i - \theta_j) + G_{ij} v_i v_j \sin(\theta_i - \theta_j) \right)^2 \leq S_{ij}^2 \quad \forall (i, j) \in \mathcal{L}, \end{aligned} \quad (3)$$

$$\begin{aligned} & \left(-G_{jj} v_j^2 + G_{ji} v_j v_i \cos(\theta_j - \theta_i) + B_{ji} v_j v_i \sin(\theta_j - \theta_i) \right)^2 \\ & + \left(B_{jj} v_j^2 - B_{ji} v_j v_i \cos(\theta_j - \theta_i) + G_{ji} v_j v_i \sin(\theta_j - \theta_i) \right)^2 \leq S_{ij}^2 \quad \forall (i, j) \in \mathcal{L}, \end{aligned} \quad (4)$$

$$\underline{\mathbf{V}} \leq \mathbf{v} \leq \overline{\mathbf{V}}, \quad \underline{\mathbf{P}} \leq \mathbf{p} \leq \overline{\mathbf{P}}, \quad \underline{\mathbf{Q}} \leq \mathbf{q} \leq \overline{\mathbf{Q}}, \quad \underline{\boldsymbol{\theta}} \leq \boldsymbol{\theta} \leq \overline{\boldsymbol{\theta}}. \quad (5)$$

Similarly, the power flow limit constraints (3) and (4) are convex quadratic in c_{ij} and s_{ij} :

$$\begin{aligned} & \left(-G_{ii} c_{ii} + G_{ij} c_{ij} - B_{ij} s_{ij} \right)^2 \\ & + \left(B_{ii} c_{ii} - B_{ij} c_{ij} - G_{ij} s_{ij} \right)^2 \leq S_{ij}^2 \quad \forall (i, j) \in \mathcal{L}, \end{aligned} \quad (12)$$

$$\begin{aligned} & \left(-G_{jj} c_{jj} + G_{ji} c_{ij} + B_{ji} s_{ij} \right)^2 \\ & + \left(B_{jj} c_{jj} - B_{ji} c_{ij} + G_{ji} s_{ij} \right)^2 \leq S_{ij}^2 \quad \forall (i, j) \in \mathcal{L}. \end{aligned} \quad (13)$$

The box constraints (5) are reformulated as follows:

$$\begin{aligned} & \underline{V}_i^2 \leq c_{ii} \leq \overline{V}_i^2 \quad \forall i \in \mathcal{B}, \\ & \underline{\mathbf{P}} \leq \mathbf{p} \leq \overline{\mathbf{P}}, \quad \underline{\mathbf{Q}} \leq \mathbf{q} \leq \overline{\mathbf{Q}}, \quad \underline{\boldsymbol{\theta}} \leq \boldsymbol{\theta} \leq \overline{\boldsymbol{\theta}}. \end{aligned} \quad (14)$$

As a result, an equivalent formulation for the AC-OPF model \mathcal{P}_{opt} is:

$$\mathcal{P}_{opt}^{cs\theta} : \min_{(\mathbf{p}, \mathbf{q}, \mathbf{c}, \mathbf{s}, \boldsymbol{\theta})} f(\mathbf{p}) \quad \text{s.t. (8) - (14)}. \quad (15)$$

With this reformulation, the decisions are $\mathbf{x} = (\mathbf{p}, \mathbf{q}, \mathbf{c}, \mathbf{s}, \boldsymbol{\theta})$. Constraints (10) – (14) define a convex set. We also have two non-convex equality constraints:

- Constraints (8): $c_{ij}^2 + s_{ij}^2 - c_{ii} c_{jj} = 0$, $\forall (i, j) \in \mathcal{L}$. We will refer to them as *quadratic* constraints.
- Constraints (9): $\sin(\theta_i - \theta_j) c_{ij} + \cos(\theta_i - \theta_j) s_{ij} = 0$, $\forall (i, j) \in \mathcal{L}$. We will refer to them as *trigonometric* constraints.

III. OPTIMIZATION ALGORITHM AND ITS CONVERGENCE GUARANTEES

In this section, we cast the quadratic formulation (15) of the AC-OPF model as a generic non-convex optimization problem with nonlinear equality constraints, propose an exact penalty reformulation, and solve it using a Gauss-Newton-type algorithm. We further characterize global convergence rate of our algorithm. The proofs of all theoretical results are provided in Appendices A and B.

A. Constrained NLP formulation of Optimal Power Flow

Problem $\mathcal{P}_{opt}^{cs\theta}$ can be written in the following generic form:

$$\begin{cases} \min_{\mathbf{x}=(\mathbf{p}, \mathbf{q}, \mathbf{c}, \mathbf{s}, \boldsymbol{\theta})} f(\mathbf{p}) \\ \text{s.t. } \Lambda(\mathbf{p}, \mathbf{q}, \mathbf{c}, \mathbf{s}) = 0, \quad \Psi(\mathbf{c}, \mathbf{s}, \boldsymbol{\theta}) = 0, \\ \underline{\mathbf{X}} \leq \mathbf{x} \leq \overline{\mathbf{X}}, \quad \mathbf{x}^\top \mathbf{H}_{ij} \mathbf{x} \leq S_{ij}^2 \quad (i, j) \in \mathcal{L}, \end{cases} \quad (16)$$

where f is a convex function; Λ is a linear operator defining the balance equations (10) and (11); Ψ collects all the quadratic equality constraints from (8) and the trigonometric equality constraints (9); $\underline{\mathbf{X}}$ and $\overline{\mathbf{X}}$ are given lower bounds and upper bounds on \mathbf{x} , respectively; and \mathbf{H}_{ij} are positive semi-definite matrices, with the associated constraints representing the line flow limits (12) and (13).

To provide a unified theoretical study for (16), we rewrite it in the following compact form:

$$\min_{\mathbf{x} \in \mathbb{R}^d} f(\mathbf{x}) \quad \text{s.t. } \Psi(\mathbf{x}) = 0, \quad \mathbf{x} \in \Omega, \quad (17)$$

where, in the context of AC-OPF, we have $\mathbf{x} := (\mathbf{p}, \mathbf{q}, \mathbf{c}, \mathbf{s}, \boldsymbol{\theta})$, $f(\mathbf{x}) := f(\mathbf{p})$, $\Psi(\mathbf{x}) := \Psi(\mathbf{c}, \mathbf{S}, \boldsymbol{\theta})$, and

$$\Omega := \left\{ \mathbf{x} \in \mathbb{R}^d \mid \Lambda(\mathbf{c}, \mathbf{s}, \mathbf{p}, \mathbf{q}) = 0, \quad \underline{\mathbf{X}} \leq \mathbf{x} \leq \overline{\mathbf{X}}, \quad \mathbf{x}^\top \mathbf{H}_{ij} \mathbf{x} \leq S_{ij}^2 \quad (i, j) \in \mathcal{L} \right\}. \quad (18)$$

Hence, in the sequel we devise an algorithm for solving the non-convex optimization problem (17). For this problem we assume throughout this section that the objective function f is convex and differentiable, Ω is a compact convex set, and the non-convexity enters in (17) through the non-linear equality constraints $\Psi(\mathbf{x}) = 0$. We further assume that Ψ is differentiable and its Jacobian Ψ' is Lipschitz continuous, i.e. there exists $L_\Psi > 0$ such that:

$$\|\Psi'(\mathbf{x}) - \Psi'(\hat{\mathbf{x}})\| \leq L_\Psi \|\mathbf{x} - \hat{\mathbf{x}}\| \quad \forall \mathbf{x}, \hat{\mathbf{x}} \in \Omega.$$

$\|\cdot\|$ is the ℓ_2 -norm. Note that all these assumptions hold for the AC-OPF problem (16). Indeed, f is quadratic, and since $\Lambda(\cdot)$ is linear, $\underline{\mathbf{X}} \leq \mathbf{x} \leq \overline{\mathbf{X}}$ are boxes, and $\mathbf{x}^\top \mathbf{H}_{ij} \mathbf{x} \leq S_{ij}^2$ $\forall (i, j) \in \mathcal{L}$ is convex, Ω is a closed, convex, and bounded

set. Moreover, since Ψ is the collection of (8) and (9), we show in the next lemma that it is differentiable and that its Jacobian is Lipschitz continuous.

Lemma III.1. *For the AC-OPF problem, Ψ defined by (8)–(9), is smooth, and its Jacobian Ψ' is Lipschitz continuous with a Lipschitz constant L_Ψ , i.e. $\|\Psi'(\mathbf{x}) - \Psi'(\hat{\mathbf{x}})\| \leq L_\Psi \|\mathbf{x} - \hat{\mathbf{x}}\|$ for all $\mathbf{x}, \hat{\mathbf{x}} \in \Omega$, where*

$$L_\Psi := \max \left\{ 2, (1 + 2 \max \{ \bar{V}_i^2 \mid i \in \mathcal{B} \})^{1/2} \right\} < +\infty. \quad (19)$$

Further, let \mathcal{N}_Ω defines the normal cone of Ω as

$$\mathcal{N}_\Omega(\mathbf{x}) := \begin{cases} \{ \mathbf{w} \in \mathbb{R}^d \mid \mathbf{w}^\top (\mathbf{y} - \mathbf{x}) \geq 0, \mathbf{y} \in \Omega \}, & \text{if } \mathbf{x} \in \Omega \\ \emptyset, & \text{otherwise.} \end{cases}$$

Since problem (17) is nonconvex, our goal is to search for a stationary point of (17) that is a candidate of local optima in the following sense.

Definition III.1. *A point $(\mathbf{x}^*, \mathbf{y}^*)$ is said to be a KKT point of (17) if it satisfies the following conditions:*

$$0 \in \nabla f(\mathbf{x}^*) + \Psi'(\mathbf{x}^*)\mathbf{y}^* + \mathcal{N}_\Omega(\mathbf{x}^*), \quad \mathbf{x}^* \in \Omega, \quad \Psi(\mathbf{x}^*) = 0. \quad (20)$$

Here, \mathbf{x}^* is called a stationary point of (17), and \mathbf{y}^* is the corresponding multiplier. Let \mathcal{S}^* denote the set of these stationary points.

Since Ω is compact, and Ψ and f are continuous, by the well-known Weierstrass theorem, we have:

Proposition III.1. *If $\Omega \cap \{ \mathbf{x} \mid \Psi(\mathbf{x}) = 0 \} \neq \emptyset$, then (17) has global optimal solutions.*

B. Exact penalized formulation

Associated with (17), we consider its exact penalty form:

$$\min_{\mathbf{x} \in \Omega} \left\{ F(\mathbf{x}) := f(\mathbf{x}) + \beta |\Psi(\mathbf{x})| \right\}, \quad (21)$$

where $\beta > 0$ is a penalty parameter, and $|\cdot|$ is the ℓ_1 -norm.

Two reasons for choosing an exact (non-smooth) penalty are as follows. First, for a certain finite choice of the parameter β , a single minimization in x of (21) can yield an exact solution of the original problem (17). Second, it does not square the condition number of Ψ as in the case of quadratic penalty methods, thus making our algorithm presented below more robust to ill-conditioning of the non-convex constraints. Now, we summarize the relationship between stationary points of (17) and of its penalty form (21). For this, let us define:

$$DF(\mathbf{x}^*)[\mathbf{d}] := \nabla f(\mathbf{x}^*)^\top \mathbf{d} + \beta \xi(\mathbf{x}^*)^\top \Psi'(\mathbf{x}^*)^\top \mathbf{d}, \quad (22)$$

where $\xi(\mathbf{x}^*) \in \partial |\Psi(\mathbf{x}^*)|$ is one subgradient of $|\cdot|$ at $\Psi(\mathbf{x}^*)$, and $\partial |\cdot|$ denotes the subdifferential of $|\cdot|$, see [20]. Recall that the necessary optimality condition of (21) is

$$0 \in \nabla f(\mathbf{x}^*) + \beta \Psi'(\mathbf{x}^*) \partial |\Psi(\mathbf{x}^*)| + \mathcal{N}_\Omega(\mathbf{x}^*).$$

Then, this condition can be expressed equivalently as

$$DF(\mathbf{x}^*)[\mathbf{d}] \geq 0, \quad \forall \mathbf{d} \in \mathcal{F}_\Omega(\mathbf{x}^*), \quad (23)$$

where $\mathcal{F}_\Omega(\mathbf{x})$ is the set of feasible directions to Ω at \mathbf{x} :

$$\mathcal{F}_\Omega(\mathbf{x}) := \{ \mathbf{d} \in \mathbb{R}^d \mid \mathbf{d} = t(\mathbf{y} - \mathbf{x}), \mathbf{y} \in \Omega, t \geq 0 \}. \quad (24)$$

Any point \mathbf{x}^* satisfying (23) is called a stationary point of the penalized problem (21). If, in addition, \mathbf{x}^* is feasible to (17), then we say that \mathbf{x}^* is a feasible stationary point. Otherwise, we say that \mathbf{x}^* is an infeasible stationary point.

Proposition III.2 shows the relation between (17) and (21).

Proposition III.2 ([15], (Theorem 17.4.)). *Suppose that \mathbf{x}^* is a feasible stationary point of (21) for β sufficiently large. Then, \mathbf{x}^* is also stationary point of the original problem (17).*

In general, β needs to be chosen such that $\beta > \|\mathbf{y}^*\|_\infty$, where \mathbf{y}^* is any optimal Lagrange multiplier of (17). We will discuss in detail the choice of β in Section IV.

C. Global and robust Gauss-Newton method

We first develop our GN algorithm. Then, we investigate its global convergence rate.

1) *The derivation of the Gauss-Newton scheme and the full algorithm:* Our GN method aims at solving the penalized problem (21) using the following convex subproblem:

$$\min_{\mathbf{x} \in \Omega} \left\{ \begin{aligned} \mathcal{Q}_L(\mathbf{x}; \mathbf{x}^k) &:= f(\mathbf{x}) \\ &+ \beta |\Psi(\mathbf{x}^k) + \Psi'(\mathbf{x}^k)(\mathbf{x} - \mathbf{x}^k)| + \frac{L}{2} \|\mathbf{x} - \mathbf{x}^k\|^2 \end{aligned} \right\}, \quad (25)$$

where \mathbf{x}^k is a given point in Ω for linearization, $\Psi'(\cdot)$ is the Jacobian of Ψ , and $L > 0$ is a regularization parameter. Note that our subproblem (25) differs from those used in classical penalty methods [15], since we linearize the constraints and we also add a regularization term. Thus, the objective function of (25) is strongly convex. Hence, if Ω is nonempty, this problem admits a unique optimal solution, and can be solved efficiently by several convex methods and solvers. Let us denote

$$\mathbf{V}_L(\mathbf{x}^k) := \operatorname{argmin}_{\mathbf{x} \in \Omega} \left\{ \begin{aligned} \mathcal{Q}_L(\mathbf{x}; \mathbf{x}^k) &:= f(\mathbf{x}) \\ &+ \beta |\Psi(\mathbf{x}^k) + \Psi'(\mathbf{x}^k)(\mathbf{x} - \mathbf{x}^k)| + \frac{L}{2} \|\mathbf{x} - \mathbf{x}^k\|^2 \end{aligned} \right\}. \quad (26)$$

The necessary and sufficient optimality condition for subproblem (25) becomes

$$\begin{aligned} [\nabla f(\mathbf{V}_L(\mathbf{x}^k)) + L(\mathbf{V}_L(\mathbf{x}^k) - \mathbf{x}^k) \\ + \beta \Psi'(\mathbf{x}^k) \xi(\mathbf{x}^k)]^\top (\hat{\mathbf{x}} - \mathbf{V}_L(\mathbf{x}^k)) \geq 0, \quad \forall \hat{\mathbf{x}} \in \Omega, \end{aligned} \quad (27)$$

where $\xi(\mathbf{x}^k) \in \partial |\Psi(\mathbf{x}^k) + \Psi'(\mathbf{x}^k)(\mathbf{V}_L(\mathbf{x}^k) - \mathbf{x}^k)|$.

Given $\mathbf{V}_L(\mathbf{x}^k)$, we define the following quantities:

$$\begin{aligned} \mathbf{G}_L(\mathbf{x}^k) &:= L(\mathbf{x}^k - \mathbf{V}_L(\mathbf{x}^k)), \quad \mathbf{d}_L(\mathbf{x}^k) := \mathbf{V}_L(\mathbf{x}^k) - \mathbf{x}^k, \\ \text{and } r_L(\mathbf{x}^k) &:= \|\mathbf{d}_L(\mathbf{x}^k)\|. \end{aligned} \quad (28)$$

Then, $\mathbf{G}_L(\cdot)$ can be considered as a gradient mapping of F in (21) [20], and $\mathbf{d}_L(\mathbf{x}^k)$ is a search direction for Algorithm 1. As we will see later, L should be chosen such that $0 < L \leq \beta L_\Psi$.

Now, using the subproblem (25) as a main component, we can describe our GN scheme in Algorithm 1.

The main step of Algorithm 1 is the solution of (25) at Step 4. As mentioned, this problem is strongly convex, and can be solved by several methods that converge linearly. If we choose $L_k \equiv L \geq \beta L_\Psi$, then we do not need to perform a line-search on L at Step 4, and only need to solve (25) once. However, the global upper bound βL_Ψ may be too conservative, i.e. it does not take into account the

Algorithm 1 (*The Basic Global Gauss-Newton Algorithm*)

- 1: **Initialization:** Choose $\mathbf{x}^0 \in \Omega$ and a penalty parameter $\beta > 0$ sufficiently large (ideally, $\beta > \|\mathbf{y}^*\|_\infty$).
 - 2: Choose a lower bound $L_{\min} \in (0, \beta L_\psi]$.
 - 3: **For** $k := 0$ **to** k_{\max} **perform**
 - 4: Find $L_k \in [L_{\min}, \beta L_\psi]$ such that $F(\mathbf{V}_{L_k}(\mathbf{x}^k)) \leq \mathcal{Q}_{L_k}(\mathbf{V}_{L_k}(\mathbf{x}^k); \mathbf{x}^k)$ (see Lemma III.3).
 - 5: Update $\mathbf{x}^{k+1} := \mathbf{V}_{L_k}(\mathbf{x}^k)$.
 - 6: Update β if necessary.
 - 7: **End for**
-

local structures of nonlinear functions in (21). Therefore, we propose to perform a line-search in order to find an appropriate L_k . If we perform a bi-section, then the number of line-search iterations is at most $\log_2(\beta L_\psi - L_{\min})$, see [20]. The penalty parameter β can be fixed or can be updated gradually.

2) *Global convergence analysis:* We first summarize some properties of Algorithm 1 without updating β as follows.

Lemma III.2. *Let \mathbf{V}_L be defined by (26), and \mathbf{G}_L , \mathbf{d}_L , and r_L be defined by (28). Then the following statements hold:*

- (a) *If $\mathbf{V}_{L_k}(\mathbf{x}^k) = \mathbf{x}^k$, then \mathbf{x}^k is a stationary point of (21).*
- (b) *The norm $\|\mathbf{G}_{L_k}(\mathbf{x}^k)\|$ is nondecreasing in L_k , and $r_{L_k}(\mathbf{x}^k)$ is nonincreasing in L_k . Moreover, we have*

$$F(\mathbf{x}^k) - \mathcal{Q}_{L_k}(\mathbf{V}_{L_k}(\mathbf{x}^k); \mathbf{x}^k) \geq \frac{L_k}{2} r_{L_k}^2(\mathbf{x}^k). \quad (29)$$

- (c) *If $\Psi(\cdot)$ is Lipschitz continuous with the Lipschitz constant L_Ψ , then, for any $x \in \Omega$, we have*

$$\begin{aligned} F(\mathbf{x}^k) - F(\mathbf{V}_{L_k}(\mathbf{x}^k)) &\geq \frac{(2L_k - \beta L_\Psi)}{2} r_{L_k}^2(\mathbf{x}^k) \\ &= \frac{(2L_k - \beta L_\Psi)}{2L_k^2} \|\mathbf{G}_{L_k}(\mathbf{x}^k)\|^2. \end{aligned} \quad (30)$$

$$\begin{aligned} DF(\mathbf{x}^k)[\mathbf{d}_{L_k}(\mathbf{x}^k)] &\leq -L_k r_{L_k}^2(\mathbf{x}^k) \\ &= -\frac{1}{L_k} \|\mathbf{G}_{L_k}(\mathbf{x}^k)\|^2. \end{aligned}$$

Statement (a) shows that if we can find \mathbf{x}^k such that $\|\mathbf{G}_{L_k}(\mathbf{x}^k)\| \leq \varepsilon$, then \mathbf{x}^k is an approximate stationary point of (21) within the accuracy ε . From statement (b), we can see that if the line-search condition $F(\mathbf{V}_{L_k}(\mathbf{x}^k)) \leq \mathcal{Q}_{L_k}(\mathbf{V}_{L_k}(\mathbf{x}^k); \mathbf{x}^k)$ at Step 4 holds, then $F(\mathbf{V}_{L_k}(\mathbf{x}^k)) \leq F(\mathbf{x}^k) - \frac{L_k}{2} r_{L_k}^2(\mathbf{x}^k)$. That is, the objective value $F(\mathbf{x}^k)$ decreases at least by $\frac{L_k}{2} r_{L_k}^2(\mathbf{x}^k)$ after the k -th iteration. We first claim that Algorithm 1 is well-defined.

Lemma III.3. *Algorithm 1 is well-defined, i.e. step 4 terminates after a finite number of iterations. That is, if $L \geq \beta L_\Psi$, then $F(\mathbf{V}_L(\mathbf{x}^k)) \leq \mathcal{Q}_L(\mathbf{V}_L(\mathbf{x}^k); \mathbf{x}^k)$.*

Let $\mathcal{L}_F(\alpha) = \{x : F(x) \leq \alpha\}$ be the level set of F at α . Now, we are ready to state the following theorem on global convergence of Algorithm 1.

Theorem III.1. *Suppose that the feasible set \mathcal{F} is sufficiently large such that $\mathcal{L}_F(F(\mathbf{x}^k)) \subset \mathcal{F}$ for $k \geq 0$. Then, the sequence $\{\mathbf{x}^k\}$ generated by Algorithm 1 satisfies*

$$\min_{0 \leq k \leq K} \|\mathbf{G}_{\beta L_\Psi}(\mathbf{x}^k)\|^2 \leq \frac{2(\beta L_\Psi)^2}{L_{\min}(K+1)} [F(\mathbf{x}^0) - F^*], \quad (31)$$

where $F^* := \inf_{\mathbf{x} \in \Omega} F(\mathbf{x}) > -\infty$. Moreover, we also obtain

$$\lim_{k \rightarrow \infty} \|\mathbf{x}^{k+1} - \mathbf{x}^k\| = 0, \quad \text{and} \quad \lim_{k \rightarrow \infty} \|\mathbf{G}_{\beta L_\Psi}(\mathbf{x}^k)\| = 0, \quad (32)$$

and the set of limit points \hat{S}^* of the sequence $\{\mathbf{x}^k\}_{k \geq 0}$ is connected. If this sequence is bounded (in particular, if $\mathcal{L}_F(F(\mathbf{x}^0))$ is bounded) then every limit point is a stationary point of (21). Moreover, if the set of limit points \hat{S}^* is finite, then the sequence $\{\mathbf{x}^k\}$ converges to a stationary point $\mathbf{x}^* \in S^*$ of (21). If, in addition, \mathbf{x}^* is feasible to (17) and β is sufficiently large, then \mathbf{x}^* is also a stationary point of (17).

Theorem III.1 provides a global convergence result for Algorithm 1. Moreover, our algorithm requires solving convex subproblems at each iteration, thus offering a great advantage over classical penalty-type schemes. However, we only show that, under the stated conditions, the iterate sequence $\{\mathbf{x}^k\}$ converges to a stationary point \mathbf{x}^* of (21). Since $\mathbf{x}^* \in \Omega$, if $\Psi(\mathbf{x}^*) = 0$, then \mathbf{x}^* is also a stationary point of (17). We can guarantee this by combining the algorithm with a *run-and-inspect procedure*, whereby if \mathbf{x}^* violates $\Psi(\mathbf{x}) = 0$, then we restart the algorithm at a new starting point. However, we leave this extension for our future work.

IV. IMPLEMENTATION & SIMULATION

In this section, we benchmark the GN algorithm against MATPOWER instances that are solved using IPOPT, which is a state-of-the-art interior-point solver. We consider transmission networks with sizes ranging from 1,354 buses to 25,000 buses. Our first goal is to optimize the settings of the GN method. We will see that the choice of β and L is crucial. This will allow us to derive a practical version of the GN algorithm, which we compare to IPOPT.

A. A Practical Implementation of Algorithm 1 for AC-OPF

1) *Subproblem (26) in the context of AC-OPF:* We first recall how the AC-OPF formulation $\mathcal{P}_{opt}^{cs\theta}$ can be cast in our GN framework by specifying the following components:

- $\mathbf{x} := (\mathbf{p}, \mathbf{q}, \mathbf{c}, \mathbf{s}, \boldsymbol{\theta})$, $f(\mathbf{x}) = f(\mathbf{p})$.
- $\Psi(\mathbf{x}) = \begin{cases} \Psi_q^{ij}(\mathbf{c}, \mathbf{s}) = c_{ij}^2 + s_{ij}^2 - c_{ii}c_{jj} \\ \Psi_t^{ij}(\mathbf{c}, \mathbf{s}, \boldsymbol{\theta}) = \sin(\theta_i - \theta_j)c_{ij} + \cos(\theta_i - \theta_j)s_{ij} \end{cases}$
 $\forall (i, j) \in \mathcal{L}$.
- $\Omega := \{\mathbf{x} \in \mathbb{R}^p \mid \mathbf{x} \text{ satisfies (10), (11), (12), (13), (14)}\}$.

We define the following functions in order to keep our notation compact:

$$\begin{aligned} \Phi_q(\mathbf{c}, \mathbf{s}, \mathbf{dc}, \mathbf{ds}) &= \sum_{(i,j) \in \mathcal{L}} |\Psi_q^{ij}(\mathbf{c}, \mathbf{s}) + \Psi_q^{ij'}(\mathbf{c}, \mathbf{s})(\mathbf{dc}, \mathbf{ds})^\top|, \\ \Phi_t(\mathbf{c}, \mathbf{s}, \boldsymbol{\theta}, \mathbf{dc}, \mathbf{ds}, \mathbf{d}\boldsymbol{\theta}) &= \sum_{(i,j) \in \mathcal{L}} |\Psi_t^{ij}(\mathbf{c}, \mathbf{s}, \boldsymbol{\theta}) + \Psi_t^{ij'}(\mathbf{c}, \mathbf{s}, \boldsymbol{\theta})(\mathbf{dc}, \mathbf{ds}, \mathbf{d}\boldsymbol{\theta})^\top|. \end{aligned}$$

Note that we have two different type of constraints (*quadratic and trigonometric*) and that they may attain different relative scales for different instances, as it is the case in our numerical experiments. We will define different penalty terms depending on the type of constraint, which will increase the flexibility of our implementation, whereas it does not affect our theory. To

this end, we denoted by β_q (resp. β_t) the β penalty parameter associated with the quadratic (resp. trigonometric) constraints. The trigonometric constraints depend on \mathbf{c} , \mathbf{s} and $\boldsymbol{\theta}$, whereas the quadratic ones only depend on \mathbf{c} and \mathbf{s} . Therefore, we define two separate regularization parameters: L_{cs} and L_θ (we drop the k subindex from now on for notational simplicity).

The GN subproblem at iteration k , corresponding to (25), is convex and has the form:

$$\begin{aligned} \mathcal{P}_{sub}^k : \quad & \min_{(\mathbf{y}, \mathbf{d})} \quad f(\mathbf{p}) + \beta_q \Phi_q(\mathbf{c}^k, \mathbf{s}^k, \mathbf{dc}, \mathbf{ds}) \\ & + \beta_t \Phi_t(\mathbf{c}^k, \mathbf{s}^k, \boldsymbol{\theta}^k, \mathbf{dc}, \mathbf{ds}, \mathbf{d}\boldsymbol{\theta}) \\ & + \frac{L_{cs}}{2} \|(\mathbf{dc}, \mathbf{ds})\|^2 + \frac{L_\theta}{2} \|\mathbf{d}\boldsymbol{\theta}\|^2 \\ \text{s.t.} \quad & \mathbf{y} = (\mathbf{p}, \mathbf{q}), \quad \mathbf{d} = (\mathbf{dc}, \mathbf{ds}, \mathbf{d}\boldsymbol{\theta}) \\ & (\mathbf{p}, \mathbf{q}, \mathbf{c}^k + \mathbf{dc}, \mathbf{s}^k + \mathbf{ds}, \boldsymbol{\theta}^k + \mathbf{d}\boldsymbol{\theta}) \in \Omega. \end{aligned}$$

The optimal solution of \mathcal{P}_{sub}^k , which we denote by $(\mathbf{y}^*, \mathbf{d}^*)$, provides the next iterate $\mathbf{x}^{k+1} = (\mathbf{p}^*, \mathbf{q}^*, \mathbf{c}^k + \mathbf{dc}^*, \mathbf{s}^k + \mathbf{ds}^*, \boldsymbol{\theta}^k + \mathbf{d}\boldsymbol{\theta}^*)$.

2) *Stopping criteria*: We terminate Algorithm 1 in three occasions, which, in our experiments, work quite reasonably:

- If the maximum number of iterations $k_{\max} := 100$ has been reached, we terminate our experiments.
- If the difference $\|\mathbf{x}^{k+1} - \mathbf{x}^k\|_\infty < \epsilon_1$, then Algorithm 1 has reached an approximate stationary point of the exact penalized formulation (21) (see Lemma III.2(a)), and we also terminate Algorithm 1. However, in this case it is possible that the last iterate might not be feasible for $\mathcal{P}_{opt}^{cs\theta}$. We numerically check the feasibility of $\mathcal{P}_{opt}^{cs\theta}$ by directly computing the feasibility violation. In the experiments section, we employ a value of $\epsilon_1 := 1e^{-6}$.
- If the quadratic and trigonometric constraints are satisfied with tolerance ϵ_2 , where $\epsilon := 1e^{-5}$, we also terminate. Concretely, we stop Algorithm 1 if $Feas^k := \max(\|\Psi_q(\mathbf{c}^k, \mathbf{s}^k)\|_\infty, \|\Psi_t(\mathbf{c}^k, \mathbf{s}^k, \boldsymbol{\theta}^k)\|_\infty) < \epsilon_2$.

3) *Parameter tuning strategies*: Tuning the parameters is quite crucial to improve practical performance of constrained nonconvex algorithms, including Algorithm 1. We demonstrate the impact of a careful choice for parameters in Fig. 1. This figure presents the performance of Algorithm 1 on the MATPOWER instance (case1888rte), with a constant value for β and L (i.e. $\beta_t = \beta_q = \beta$ and $L_{cs} = L_\theta = L$). Concretely, we fix $\beta = 100$ and set L to the theoretical upper bound $L = \beta \cdot L_\psi$ as described in our theory. As shown in Fig. 1, the algorithm reaches the maximum number of iterations (one hundred), but shows some slow progress on the quadratic feasibility. Although the maximum violation of the trigonometric constraints remains within the acceptable tolerance of $\epsilon_2 = 1e^{-5}$ within 6 iterations, the maximum violation of the quadratic constraints decreases very slowly without reaching the desired tolerance. This behavior reveals that a careful balance between the different parameters needs to be achieved. The cause of the poor performance in Fig. 1 is the fact that the trigonometric constraints are quickly satisfied, which ‘locks in’ the values of \mathbf{c} , \mathbf{s} , and $\boldsymbol{\theta}$, and limits the ability of the algorithm to decrease the maximum violations of the quadratic constraints. Note that this is consistent with the fact that the objective value is not evolving over iterations.

4) *Different parameter choices for two types of constraints*: Following a detailed experimental investigation which is presented in Appendix C, we fix the parameters of Algorithm 1 as follows. We set β_t equal to the number of lines in the network, $\beta_t = |\mathcal{L}|$, and we set $\beta_q = 5\beta_t$. The intuition behind these choices is that (i) according to Proposition III.2, large values of β ensure the equivalence between (17) and (21); (ii) quadratic constraints and trigonometric constraints scale up differently. Concerning the values for L_{cs} and L_θ , we perform a geometric line search at line 4 of Algorithm 1 and choose $L_{cs, \min} := 1$, $L_{\theta, \min} := 1$ and the geometric update coefficient $\mu := 2$. Since we need to solve \mathcal{P}_{sub}^k each time L_{cs} and/or L_θ are updated, keeping the number of updates of L low is crucial for the performance of the algorithm. The detailed justification of our approach towards updating the values of the L coefficient is developed in Appendix D.

B. Numerical experiments

We used the MATPOWER library in order to compare our approach to IPOPT for a wide range of test systems that have been investigated in the literature. MATPOWER provides a large set of instances of AC-OPF. We tested our approach on instances whose size ranges between 1,354 and 25,000 nodes. MATPOWER also provides several possibilities for solving AC-OPF. We benchmark our approach against IPOPT, a nonlinear solver based on the interior-point method. Since we initialize the GN algorithm with the solution of the SOCP relaxation of AC-OPF, we also initialize IPOPT with the solution of the SOCP relaxation, in order to establish a fair comparison.

We compare the following three methods:

- 1) **GN**: GN algorithm initialized at the solution of the SOCP relaxation. The parameters of the algorithm are chosen according to section IV-A4.
- 2) **MP-IPOPT**: The MATPOWER implementation of IPOPT. MATPOWER uses the midpoints of the box constraints of the problem as an initial solution for the interior-point solver.
- 3) **SOCP-IPOPT**: IPOPT initialized at the solution of the SOCP relaxation.

The results of our analysis are presented in Table I. The MATPOWER implementation of IPOPT fails in a number of instances¹. Note that the instances 1888rte, 2868rte, 6468rte, 6515rte present exceeding run times or significant constraint violations. Other test cases perform extremely well, most notably the last four instances which are also the largest ones. When we initialize IPOPT from the solution of the SOCP relaxation, the violation of the constraints is less sensitive across instances, however the variation in execution time remains significant.

We note that the GN algorithm converges in tens of iterations. Even if the GN algorithm does not always provide a solution within the target tolerance, the constraint violation never exceeds a level of 10^{-2} . For the 11 first instances, the solutions provided by GN are feasible and the run time does

¹The indication (Maximum Violation) $MV > 1e^{-5}$ in MP-IPOPT and SOCP-IPOPT implies that IPOPT reaches the maximum number of iterations.



Fig. 1. Evolution of maximum violation of the quadratic and tangent constraints, and the objective function along the iterations for case1888rte, for $\beta = 100$ and a fixed value of L along the iterations.

TABLE I
COMPARISON OF THE GN ALGORITHM AGAINST IPOPT ON 15 MATPOWER INSTANCES.

Test Case	Gauss-Newton				MP-IPOPT			SOCP-IPOPT		
	# It+L	Objective	Time	MV	Objective	Time	MV	Objective	Time	MV
1354pegase	4+0	$7.417e^4$	7.21	$9e^{-6}$	$7.407e^4$	1.59	$3e^{-6}$	$7.456e^4$	81	$5e^{-3}$
1888rte	27+28	$6.057e^4$	132	$9e^{-6}$	$5.399e^4$	3,675	$8e^{+3}$	$6.053e^4$	20.6	$2e^{-6}$
1951rte	3+0	$8.183e^4$	10.0	$3e^{-7}$	$8.174e^4$	26.8	$1e^{-6}$	$8.174e^4$	30.9	$2e^{-6}$
2383wp	16+1	$1.928e^6$	82.9	$5e^{-6}$	$1.868e^6$	3.86	$3e^{-8}$	$1.869e^6$	18.4	$2e^{-6}$
2848rte	6+0	$5.308e^4$	32.4	$1e^{-6}$	$5.302e^4$	2,604	$3e^{-4}$	$5.302e^4$	76.3	$3e^{-6}$
2868rte	5+0	$7.990e^4$	28.5	$8e^{-7}$	$5.833e^4$	3,868	$1e^{+5}$	$7.979e^4$	62.5	$2e^{-6}$
2869pegase	3+0	$1.342e^5$	20.6	$3e^{-6}$	$1.340e^5$	3.11	$1e^{-6}$	$1.349e^5$	194	$1e^{-1}$
6468rte	14+8	$8.713e^4$	607	$5e^{-6}$	$6.252e^4$	4,350	$1e^{+5}$	$8.834e^4$	372	$6e^{-4}$
6470rte	11+0	$9.856e^4$	424	$2e^{-6}$	$9.835e^4$	68.4	$1e^{-6}$	$9.995e^4$	406	$2e^{-4}$
6495rte	4+0	$1.065e^5$	157	$2e^{-6}$	$1.063e^6$	135	$4e^{-6}$	$1.074e^6$	428	$7e^{-5}$
6515rte	4+0	$1.101e^5$	163	$2e^{-6}$	$7.385e^4$	5,761	$1e^{+5}$	$1.108e^5$	466	$5e^{-4}$
9241pegase	43+41	$3.152e^5$	6,304	$3e^{-2}$	$3.159e^5$	66.4	$4e^{-6}$	$3.217e^5$	942	$3e^{-4}$
ACTIVSg10k	9+4	$2.532e^6$	974	$6e^{-6}$	$2.486e^6$	84.9	$1e^{-6}$	$2.504e^6$	901	$5e^{-3}$
13651pegase	33+35	$3.856e^5$	8,176	$2e^{-2}$	$3.861e^5$	30.2	$2e^{-6}$	$3.867e^5$	1,016	$2e^{+2}$
ACTIVSg25k	16+0	$6.114e^6$	10,484	$8e^{-6}$	$6.018e^6$	79.1	$2e^{-7}$	$6.018e^6$	1,079	$4e^{-6}$

not exceed a few hundreds of seconds. On the last 4 instances, GN encounters difficulties with the size of the subproblem. For both pegase test cases, the convergence of the algorithm is challenging. The size of the subproblems in these last four instances results in run times in the order of magnitude of thousands of seconds, whereas MP-IPOPT solves these instances in less than 100 seconds.

In our implementation, we use Gurobi as a convex solver to solve the subproblem $\mathcal{P}_{\text{sub}}^k$, which unfortunately does not allow us to exploit a warm-start strategy due to the use of interior-point methods. This is the main reason why GN takes a few iterations but its computational time is large. We strongly believe that if a warm-start strategy is injected, it will significantly improve the performance of our GN algorithm.

C. Robustness of the GN approach

In this section, we examine the robustness of the three algorithms against perturbation of input data. We select the 1951rte test case, perturb its cost function, and test the performance of GN and IPOPT for different starting points.

1) *Robustness against the perturbation of input data:* We choose the 1951rte case study since all three methods perform similarly in Table I. By default in this test case, all generators are characterized by a constant marginal cost equal to 1. For our sensitivity analysis, we perturb the marginal cost by assigning a random value² between -1 and 1 . We repeat this 3 times and obtain the test cases 1951rte_1,

²Note that negative marginal costs may correspond to price-taking units that wish to engage in bilateral trade and are therefore submitting competitive offers in order to improve their chances of being dispatched.

1951rte_2 and 1951rte_3. The results of this sensitivity analysis are presented in Table II, where we limit the execution time to 1 hour. We observe that MP-IPOPT is impacted significantly by the perturbation in terms of the Maximum Violation (MV) of the constraints. SOCP-IPOPT fails to converge to a point within the desired tolerance for 1951rte_2 and 1951rte_3 even if its execution time is only slightly increased. The execution time and the number of iterations of the GN method increases, nevertheless, the algorithm achieves a robust performance compared to IPOPT.

TABLE II
COMPARISON OF GN VERSUS IPOPT ON THE 1951RTE INSTANCE AND THREE PERTURBED VERSIONS OF 1951RTE WHERE MARGINAL COSTS HAVE BEEN PERTURBED.

Test Case	Gauss-Newton			MP-IPOPT		SOCP-IPOPT	
	# It+L	Time	MV	Time	MV	Time	MV
1951rte	3+0	10.0	$3e^{-7}$	26.8	$1e^{-6}$	30.9	$2e^{-6}$
1951rte_1	17+5	129	$6e^{-6}$	3,600	$8e^{+3}$	147	$2e^{-6}$
1951rte_2	11+5	70	$9e^{-6}$	3,600	$6e^{+4}$	126	$4e^{-3}$
1951rte_3	15+6	80	$3e^{-6}$	142	$7e^{+2}$	119	$1e^{-2}$

2) *Robustness against the choice of starting point:* In this sensitivity analysis, we initialize the algorithms from the following starting point \hat{x} :

$$\hat{p} := \frac{\bar{P} - \underline{P}}{2}, \quad \hat{q} := \frac{\bar{Q} - \underline{Q}}{2}, \quad \hat{\theta} := \frac{\bar{\theta} - \underline{\theta}}{2},$$

$$\hat{c}_{ii} := \frac{\bar{V}_{ii}^2 - \underline{V}_{ii}^2}{2}, \quad \forall i \in \mathcal{B},$$

$$\hat{c}_{ij} := \sqrt{c_{ii}c_{jj}}, \quad \hat{s}_{ij} := 0 \quad \forall (i, j) \in \mathcal{L}.$$

This initialization is inspired by initializing at the mid-point of the box constraints while ensuring that the violation of the

quadratic constraint (8) is not severe. This initialization ensures that the starting point of the algorithm is not completely meaningless for the problem at hand.

The results are presented in Table III. With the exception of 2848rte, the number of iterations for the GN methods remains in the same order of magnitude, and the violation of the constraints is comparable to the results of Table I. The GN method now solves the 9241pegase instance within a much smaller run time compared to the case where it was being initialized with the solution of the SOCP relaxation. IPOPT fails to provide a solution within the desired tolerance in most of the cases.

TABLE III
COMPARISON OF GN VERSUS IPOPT ON 15 MATPOWER INSTANCES
WITH A DIFFERENT STARTING POINT.

Test Case	Gauss-Newton				IPOPT		
	# It+L	Objective	Time	MV	Objective	Time	MV
1354pegase	6+0	7.438e ⁴	10.3	8e ⁻⁶	7.467e ⁴	26.5	2e ⁻³
1888rte	16+15	6.058e ⁴	110	9e ⁻⁶	6.035e ⁴	127	3e ⁻³
1951rte	4+0	8.190e ⁴	21.7	2e ⁻⁶	8.174e ⁴	103	3e ⁻²
2383wp	17+0	1.916e ⁶	86.2	9e ⁻⁶	1.850e ⁶	39.9	2e ⁻⁶
2848rte	40+38	5.667e ⁴	437	3e ⁻⁴	5.314e ⁴	140	9e ⁻³
2868rte	5+0	8.001e ⁴	37.1	7e ⁻⁶	8.011e ⁴	152	4e ⁻⁷
2869pegase	7+0	1.351e ⁵	60.2	8e ⁻⁶	1.352e ⁵	252	4e ⁻³
6468rte	13+8	8.729e ⁴	401	9e ⁻⁶	8.987e ⁴	241	2e ⁻⁶
6470rte	9+0	9.869e ⁴	329	4e ⁻⁶	1.002e ⁵	439	3e ⁻⁴
6495rte	4+0	1.067e ⁵	125	8e ⁻⁶	1.080e ⁶	445	3e ⁻²
6515rte	4+0	1.102e ⁵	129	1e ⁻⁶	1.110e ⁵	450	2e ⁻³
9241pegase	7+0	3.169e ⁵	703	1e ⁻⁶	3.193e ⁵	937	6e ⁻⁴
ACTIVSg10k	14+7	2.515e ⁶	2,234	3e ⁻⁶	2.482e ⁶	893	1e ⁰
13651pegase	16+11	6.035e ⁵	4,065	3e ⁰	3.890e ⁵	970	2e ⁻²
ACTIVSg25k	7+0	6.146e ⁶	4,369	1e ⁻⁴	6.018e ⁶	838	7e ⁻⁶

V. CONCLUSION

Motivated by the increasing interest in integrating transmission and distribution system operations, in this paper we aim at tackling the AC-OPF as a non-convex optimization problem in order to recover physically implementable dispatch solutions. For medium-voltage distribution systems, DC approximations of optimal power flow are not adequate, and convex relaxations require assumptions for exactness that are often violated in practical problems.

We propose a Gauss-Newton method for resolving the problem, which relies on the quadratic reformulation of AC-OPF. We establish a global convergence rate guarantee for our algorithm. We then adapt the theory to practical applications, by testing a wide range of large-scale problems with thousands to tens of thousands of nodes that are sourced from the MATPOWER database. We compare our approach with IPOPT, which is a state-of-the-art solver that is commonly considered in the literature as a benchmark. We demonstrate comparable performance: (i) we outperform IPOPT for certain (but not all) instances, and (ii) we demonstrate improved robustness of our approach with respect to changes in the cost coefficients of the problem and changes in the starting point of the algorithm.

Ultimately, our goal is to use the proposed algorithm as a module in a heuristic scheme that can incorporate binary variables. The required adaptations to the GN algorithm towards this aim will be described in future research. The fact that our approach achieves comparable performance to an industrial off-the-shelf solver on large-scale instances is a highly encouraging step in this direction.

REFERENCES

- [1] J. Carpentier. "Contribution a l'etude du dispatching economique," *Bulletin de la Societe Francaise des Electriciens*, 3(1):431-447, 1962.
- [2] S. Frank, I. Steponavice and S. Rebennack, "Optimal power flow: a bibliographic survey," *Energy Systems*, vol. 3, no. 3, pp. 221-258, 2012.
- [3] M. B. Cain, R. P. O'Neill and A. Castillo. "History of optimal power flow and formulations", *Federal Energy Regulatory Commission*, 1-36, 2012.
- [4] H. Le Cadre, I. Mezghani and A. Papavasiliou. "A game-theoretic analysis of transmission-distribution system operator coordination", *European Journal of Operational Research*, 274(1):317-339, 2019.
- [5] J. Lavaei and S. Low, "Zero duality gap in optimal power flow problem," *IEEE Transactions on Power Systems*, vol. 27, no. 3, pp. 92-107, 2012.
- [6] B. Kocuk, S. S. Dey, and X. A. Sun. "Inexactness of SDP relaxation and valid inequalities for optimal power flow." *IEEE Transactions on Power Systems*, 31(1):642-651, 2016.
- [7] R. A. Jabr. "Optimal power flow using an extended conic quadratic formulation," *IEEE transactions on power systems*, 23(3):1000-1008, 2008.
- [8] L. Gan, N. Li, U. Topcu, and S. H. Low. "Exact convex relaxation of optimal power flow in radial networks," *IEEE Transactions on Automatic Control*, 60(1):72-87, 2015.
- [9] B. Kocuk, S. S. Dey, and X. A. Sun. "Strong soep relaxations for the optimal power flow problem," *Operations Research*, 64(6):1177-1196, 2016.
- [10] C. Coffrin, H. L. Hijazi, and P. Van Hentenryck. "The QC relaxation: A theoretical and computational study on optimal power flow," *IEEE Transactions on Power Systems*, 31(4):3008-3018, 2016.
- [11] D. K. Molzahn, J. T. Holzer, B. C. Lesieutre, and C. L. DeMarco. "Implementation of a large-scale optimal power flow solver based on semidefinite programming," *IEEE Transactions on Power Systems*, 28(4):3987-3998, 2013.
- [12] M. Caramanis, E. Ntakou, W. W. Hogan, A. Chakraborty, and J. Schoene. "Co-optimization of power and reserves in dynamic t&d power markets with nondispatchable renewable generation and distributed energy resources," *Proceedings of the IEEE*, 104(4):807-836, 2016.
- [13] I. Mezghani, A. Papavasiliou, and H. Le Cadre. "A generalized nash equilibrium analysis of electric power transmission-distribution coordination," In *e-Energy*, 526-531, 2018.
- [14] I. Mezghani and A. Papavasiliou. "A Mixed Integer Second Order Cone Program for Transmission-Distribution System Co-Optimization," *2019 IEEE Milano PowerTech*, to be published, 2019.
- [15] J. Nocedal and S. Wright. "Numerical optimization", *Springer Science & Business Media*, 2006.
- [16] C. Cartis, N.I.M. Gould, and P.L. Toint. "On the Evaluation Complexity of Composite Function Minimization with Applications to Nonconvex Nonlinear Programming", *SIAM J. Optimization*, 21(4): 1721-1739, 2011.
- [17] Y. Nesterov and B. T. Polyak. "Cubic regularization of Newton method and its global performance", *Mathematical programming*, 108(1):177-205, 2006.
- [18] Y. Dauphin, R. Pascanu, C. Gulcehre, K. Cho, S. Ganguli, and Y. Bengio. "Identifying and attacking the saddle point problem in high-dimensional non-convex optimization", In *Advances in Neural Information Processing Systems*, 2933-2941, 2014.
- [19] A. Wächter and L. T. Biegler. "On the implementation of an interior-point filter line-search algorithm for large-scale nonlinear programming", *Mathematical programming*, 106(1):25-57, 2006.
- [20] Y. Nesterov, "Modified Gauss-Newton scheme with worst case guarantees for global performance", *Optim. Methods Softw.* 22(3), 469-483, 2007.
- [21] A. G. Expósito and E. R. Ramos. "Reliable load flow technique for radial distribution networks," *IEEE Transactions on Power Systems*, 14(3):1063-1069, 1999.
- [22] R. Zimmerman, C. Murillo-Sanchez and R. Thomas, "Matpower: Steady-state operations, planning, and analysis tools for power systems research and education," *IEEE Transactions on Power Systems*, vol. 26, no. 1, pp. 12-19, 2011.
- [23] A. Eltvéd, J. Dahl, and M. S. Andersen. "On the robustness and scalability of semidefinite relaxation for optimal power flow problems," *Optimization and Engineering*, pages 1-18, 2018.

APPENDIX A
THE PROOF OF LEMMA III.1

Proof. From the definition of Ψ , it consists of two parts: quadratic forms in (c_{ij}, s_{ij}) and trigonometric and linear forms in $\theta_{ij} := \theta_i - \theta_j$ and (c_{ij}, s_{ij}) , respectively. We can write it as $\Psi = [\Psi^q, \Psi^t]$. Each function in Ψ^q has the form $c_{ij}^2 + s_{ij}^2 - c_{ii}c_{jj}$, as shown by (8), and each function in Ψ^t has the form $\sin(\theta_{ij})c_{ij} + \cos(\theta_{ij})s_{ij}$, as shown in (9). We can show that the second derivative of each component of Ψ^q w.r.t. $(c_{ii}, c_{jj}, c_{ij}, s_{ij})$ and of Ψ^t w.r.t. $(c_{ij}, s_{ij}, \theta_{ij})$, respectively is

$$\nabla^2 \Psi^q(\mathbf{x}) = \begin{bmatrix} 0 & -1 & 0 & 0 \\ -1 & 0 & 0 & 0 \\ 0 & 0 & 2 & 0 \\ 0 & 0 & 0 & 2 \end{bmatrix}, \quad \text{and}$$

$$\nabla^2 \Psi^t(\mathbf{x}) = \begin{bmatrix} 0 & 0 & \cos(\theta_{ij}) \\ 0 & 0 & -\sin(\theta_{ij}) \\ \cos(\theta_{ij}) & -\sin(\theta_{ij}) & -c_{ij} \sin(\theta_{ij}) - s_{ij} \cos(\theta_{ij}) \end{bmatrix}.$$

The second derivative $\nabla^2 \Psi^q(\mathbf{x})$ is constant. Hence, the maximum eigenvalue of $\nabla^2 \Psi^q(\mathbf{x})$ is $\lambda_{\max}(\nabla^2 \Psi^q(\mathbf{x})) = 2$. For any $\mathbf{u} := [u_1, u_2, u_3] \in \mathbb{R}^3$, we can easily estimate that

$$\begin{aligned} & \mathbf{u}^\top \nabla^2 \Psi^t(\mathbf{x}) \mathbf{u} \\ &= u_1 u_3 [-\sin(\theta_{ij}) + \cos(\theta_{ij})] + u_2 u_3 [\cos(\theta_{ij}) \\ & \quad - \sin(\theta_{ij})] + [-c_{ij} \sin(\theta_{ij}) - s_{ij} \cos(\theta_{ij})] u_3^2 \\ &\leq \frac{1}{2}(u_1^2 + u_3^2) + \frac{1}{2}(u_2^2 + u_3^2) + (|c_{ij}| + |s_{ij}|) u_3^2 \\ &\leq (1 + |c_{ij}| + |s_{ij}|)(u_1^2 + u_2^2 + u_3^2) \\ &= (1 + |c_{ij}| + |s_{ij}|) \|\mathbf{u}\|^2. \end{aligned}$$

Therefore, $\lambda_{\max}(\nabla^2 \Psi^t(\mathbf{x})) = 1 + |c_{ij}| + |s_{ij}| \leq 1 + 2 \max\{V_i^2 \mid i \in \mathcal{B}\}$, where the last inequality follows from (5). Consequently,

$$L_\Psi := \max\left\{2, (1 + 2 \max\{\bar{V}_i^2 \mid i \in \mathcal{B}\})^{1/2}\right\} < +\infty,$$

which is (19). \square

APPENDIX B
THE PROOF OF LEMMA III.2, LEMMA III.3, AND
THEOREM III.1

Proof of Lemma III.2. (a) Substituting $\mathbf{V}_{L_k}(\mathbf{x}^k) = \mathbf{x}^k$ into (27), we again obtain the optimality condition (23). This shows that \mathbf{x}^k is a stationary point of (21).

(b) Since the function $q(t, \mathbf{x}) := f(\mathbf{x}) + \beta|\Psi(\mathbf{x}^k) + \Psi'(\mathbf{x}^k)(\mathbf{x} - \mathbf{x}^k)| + \frac{1}{2t}\|\mathbf{x} - \mathbf{x}^k\|^2$ is convex in two variables \mathbf{x} and t , we have that $\eta(t) := \min_{\mathbf{x} \in \Omega} q(t, \mathbf{x})$ is still convex. It is easy to show that $\eta'(t) = -\frac{1}{2t^2}\|\mathbf{V}_{1/t}(\mathbf{x}^k) - \mathbf{x}^k\|^2 = -\frac{1}{2t^2}\|\mathbf{d}_{1/t}(\mathbf{x}^k)\|^2 = \frac{1}{2}\|\mathbf{G}_{1/t}(\mathbf{x}^k)\|^2$. Since $\eta(t)$ is convex, $\eta'(t)$ is nondecreasing in t . This implies that $\|\mathbf{G}_{1/t}(\mathbf{x}^k)\|$ is nonincreasing in t . Thus $\|\mathbf{G}_L(\mathbf{x}^k)\|$ is nondecreasing in L and $r_L(\mathbf{x}^k) := \|\mathbf{d}_L(\mathbf{x}^k)\|$ is nonincreasing in L .

To prove (29), note that the convexity of η implies that

$$F(\mathbf{x}^k) = \eta(0) \geq \eta(t) + \eta'(t)(0 - t) = \eta(t) + \frac{1}{2t} r_{1/t}^2(\mathbf{x}^k). \quad (33)$$

On the other hand, $\mathcal{Q}_L(\mathbf{V}_L(\mathbf{x}^k); \mathbf{x}^k) = \eta(1/L)$. Substituting this relation into (33), we obtain (29).

(c) Let us define $\mathbf{V}_k := \mathbf{V}_{L_k}(\mathbf{x}^k)$. From the optimality condition (27), for any $\mathbf{x} \in \Omega$, we have

$$\begin{aligned} & [\nabla f(\mathbf{V}_k) + L_k(\mathbf{V}_k - \mathbf{x}^k) + \beta\Psi'(\mathbf{x}^k)\xi(\mathbf{x}^k)]^\top (\mathbf{x} - \mathbf{V}_k) \geq 0, \\ & \text{where } \xi(\mathbf{x}^k) \in \partial|\Psi(\mathbf{x}^k) + \Psi'(\mathbf{x}^k)(\mathbf{V}_k - \mathbf{x}^k)|. \text{ Substituting } \\ & \mathbf{x} = \mathbf{x}^k \text{ into this condition, we have} \end{aligned}$$

$$\begin{aligned} \nabla f(\mathbf{V}_k)^\top (\mathbf{x}^k - \mathbf{V}_k) + \beta\xi(\mathbf{x}^k)^\top \Psi'(\mathbf{x}^k)^\top (\mathbf{x}^k - \mathbf{V}_k) \\ \geq L_k \|\mathbf{V}_k - \mathbf{x}^k\|^2. \end{aligned} \quad (34)$$

Since f and $|\cdot|$ is convex, we have

$$\begin{aligned} f(\mathbf{x}^k) & \geq f(\mathbf{V}_k) + \nabla f(\mathbf{V}_k)^\top (\mathbf{x}^k - \mathbf{V}_k) \\ |\Psi(\mathbf{x}^k)| & \geq |\Psi(\mathbf{x}^k) + \Psi'(\mathbf{x}^k)(\mathbf{V}_k - \mathbf{x}^k)| \\ & \quad + \xi(\mathbf{x}^k)^\top \Psi'(\mathbf{x}^k)^\top (\mathbf{x}^k - \mathbf{V}_k). \end{aligned}$$

Since Ψ' is Lipschitz continuous, we also have

$$\begin{aligned} |\Psi(\mathbf{V}_k)| & \leq |\Psi(\mathbf{x}^k) + \Psi'(\mathbf{x}^k)(\mathbf{V}_k - \mathbf{x}^k)| \\ & \quad + |\Psi(\mathbf{V}_k) - \Psi(\mathbf{x}^k) + \Psi'(\mathbf{x}^k)(\mathbf{V}_k - \mathbf{x}^k)| \\ & \leq |\Psi(\mathbf{x}^k) + \Psi'(\mathbf{x}^k)(\mathbf{V}_k - \mathbf{x}^k)| \\ & \quad + \frac{L_\Psi}{2} \|\mathbf{V}_k - \mathbf{x}^k\|^2. \end{aligned}$$

Combining these three estimates, we can show that

$$\begin{aligned} f(\mathbf{x}^k) + \beta|\Psi(\mathbf{x}^k)| & \geq f(\mathbf{V}_k) \\ & \quad + \beta|\Psi(\mathbf{x}^k) + \Psi'(\mathbf{x}^k)(\mathbf{V}_k - \mathbf{x}^k)| \\ & \quad + L_k \|\mathbf{V}_k - \mathbf{x}^k\|^2 \\ & \geq f(\mathbf{V}_k) + \beta|\Psi(\mathbf{V}_k)| \\ & \quad + L_k \|\mathbf{V}_k - \mathbf{x}^k\|^2 - \frac{\beta L_\Psi}{2} \|\mathbf{V}_k - \mathbf{x}^k\|^2, \end{aligned}$$

which implies

$$F(\mathbf{x}^k) \geq F(\mathbf{V}_k) + \frac{(2L_k - \beta L_\Psi)}{2} \|\mathbf{V}_k - \mathbf{x}^k\|^2.$$

Since $r_{L_k}^2(\mathbf{x}^k) = \|\mathbf{V}_k - \mathbf{x}^k\|^2 = \frac{1}{L_k^2} \|\mathbf{G}_{L_k}(\mathbf{x}^k)\|^2$, we obtain the first estimate of (30) from the last inequality.

Moreover, from (22) we have

$$\begin{aligned} DF(\mathbf{x}^k)[\mathbf{d}_{L_k}(\mathbf{x}^k)] &= \nabla f(\mathbf{V}_k)^\top (\mathbf{V}_k - \mathbf{x}^k) \\ & \quad + \beta\xi(\mathbf{x}^k)^\top \Psi'(\mathbf{x}^k)^\top (\mathbf{V}_k - \mathbf{x}^k). \end{aligned}$$

Using (34), we can show that $DF(\mathbf{x}^k)[\mathbf{d}_{L_k}(\mathbf{x}^k)] \leq -L_k \|\mathbf{V}_k - \mathbf{x}^k\|^2$, which is the second estimate of (30). \square

Proof of Lemma III.3. Since Ψ' is L_Ψ -Lipschitz continuous, for any \mathbf{x}^k and $\mathbf{V}_L(\mathbf{x}^k)$, we have

$$\begin{aligned} |\Psi(\mathbf{V}_L(\mathbf{x}^k))| & \leq |\Psi(\mathbf{x}^k) + \Psi'(\mathbf{x}^k)(\mathbf{V}_L(\mathbf{x}^k) - \mathbf{x}^k)| \\ & \quad + \|\Psi(\mathbf{V}_L(\mathbf{x}^k)) - \Psi(\mathbf{x}^k) \\ & \quad - \Psi'(\mathbf{x}^k)(\mathbf{V}_L(\mathbf{x}^k) - \mathbf{x}^k)\| \\ & \leq |\Psi(\mathbf{x}^k) + \Psi'(\mathbf{x}^k)(\mathbf{V}_L(\mathbf{x}^k) - \mathbf{x}^k)| \\ & \quad + \frac{L_\Psi}{2} \|\mathbf{V}_L(\mathbf{x}^k) - \mathbf{x}^k\|^2. \end{aligned}$$

Using the definition of $\mathcal{Q}_L(\mathbf{V}; \mathbf{x})$, we obtain

$$F(\mathbf{V}_L(\mathbf{x}^k)) \leq \mathcal{Q}_L(\mathbf{V}_L(\mathbf{x}^k); \mathbf{x}^k) - \frac{L - \beta L_\Psi}{2} \|\mathbf{V}_L(\mathbf{x}^k) - \mathbf{x}^k\|^2.$$

From this inequality, we can see that if $L \geq \beta L_\Psi$, then $F(\mathbf{V}_L(\mathbf{x}^k)) \leq \mathcal{Q}_L(\mathbf{V}_L(\mathbf{x}^k); \mathbf{x}^k)$. Hence, Step 4 of Algorithm 1 terminates after a finite number of iterations. \square

Proof of Theorem III.1. From Step 5 of Algorithm 1, we have $\mathbf{x}^{k+1} := \mathbf{V}_{L_k}(\mathbf{x}^k)$. Using (30), it is easy to obtain $-\infty < F^* \leq F(\mathbf{x}^{k+1}) \leq F(\mathbf{x}^k) \leq \dots \leq F(\mathbf{x}^0)$. This shows that $\{F(\mathbf{x}^k)\}$ is a decreasing sequence and bounded. Hence, it has at least a convergent subsequence. Moreover, from (30), we also have

$$\begin{aligned} F(\mathbf{x}^{k+1}) &\leq F(\mathbf{x}^k) - \frac{L_{\min}}{2} r_{L_k}^2(\mathbf{x}^k) \\ &\leq F(\mathbf{x}^k) - \frac{L_{\min}}{2} r_{\beta L_\psi}^2(\mathbf{x}^k). \end{aligned} \quad (35)$$

Summing up the inequality (35) from $k = 0$ to $k = K$ and using $F(\mathbf{x}^{K+1}) \geq F^*$, we obtain

$$\begin{aligned} \frac{L_{\min}}{2(\beta L_\psi)^2} \sum_{k=0}^K \|\mathbf{G}_{\beta L_\psi}(\mathbf{x}^k)\|^2 &= \frac{L_{\min}}{2} \sum_{k=0}^K r_{\beta L_\psi}^2(\mathbf{x}^k) \\ &\leq F(\mathbf{x}^0) - F(\mathbf{x}^{K+1}) \\ &\leq F(\mathbf{x}^0) - F^*. \end{aligned}$$

This implies

$$\min_{0 \leq k \leq K} \|\mathbf{G}_{\beta L_\psi}(\mathbf{x}^k)\|^2 \leq \frac{2(\beta L_\psi)^2}{L_{\min}(K+1)} [F(\mathbf{x}^0) - F^*],$$

which leads to (31). Similarly, for any $N \geq 0$ one has

$$\begin{aligned} F(\mathbf{x}^k) - F(\mathbf{x}^{k+N}) &\geq \frac{L_{\min}}{2} \sum_{i=k}^{k+N-1} r_{L_k}^2(\mathbf{x}^i) \\ &\geq \frac{L_{\min}}{2} \sum_{i=k}^{k+N-1} r_{\beta L_\psi}^2(\mathbf{x}^i). \end{aligned} \quad (36)$$

Note that the sequence $\{F(\mathbf{x}^k)\}_{k \geq 0}$ has a convergent subsequence, thus passing to the limit as $k \rightarrow \infty$ in (36) we obtain the first limit of (32). Since $\|\mathbf{x}^{k+1} - \mathbf{x}^k\| = r_{L_k}(\mathbf{x}^k) \geq r_{\beta L_\psi}(\mathbf{x}^k) = \frac{1}{\beta L_\psi} \|\mathbf{G}_{\beta L_\psi}(\mathbf{x}^k)\|$ due to Statement (b) of Lemma III.2, the first limit of (32) also implies the second one.

If the sequence $\{\mathbf{x}^k\}_{k \geq 0}$ is bounded, by passing to the limit through a subsequence and combining with Lemma III.2, we easily prove that every limit point is a stationary point of (21). If the set of limit points \mathcal{S}^* is finite. By applying the result in [1][Chapt. 28], we obtain the proof of the remaining conclusion. \square

APPENDIX C

INVESTIGATION ON PARAMETER TUNING STRATEGIES

In our first set of tests, we implement the basic variant of our method as presented in Algorithm 1 by retaining the configuration of parameters from our theoretical results. Since we only aim at validating the algorithm, we focus on the three instances that have less than 2,000 nodes: 1354pegase, 1888rte, and 1951pegase.

For the penalty parameters, we first choose the same value β for both quadratic and trigonometric constraints as $\beta = \beta^q = \beta^t$. We test with three choices of β as $\beta = 10, 100, \text{ and } 1,000$. For the regularization parameter L , we also choose the same value $L_k = L_{cs} = L_\theta$ for both L_{cs} and L_θ . We consider three different strategies when applying Algorithm 1:

- *Fixed strategy:* we fix L_k at the upper bound L_ψ , which is computed in (19).
- *Bisection update:* At each iteration k of Algorithm 1, we choose $L_{\min} = 1$ and initialize $L_k := 1$. If we do not satisfy the line-search condition $F(\mathbf{V}_{L_k}(\mathbf{x}^k)) \leq$

$\mathcal{Q}_{L_k}(\mathbf{V}_{L_k}(\mathbf{x}^k); \mathbf{x}^k)$, we apply a bisection in the interval $[L_{\min}, \beta L_\psi]$ until we satisfy this condition.

- *Geometric- μ update:* At each iteration k , we also choose $L_{\min} = 1$ and initialize $L_k := 1$. We then update $L_k \leftarrow \mu \cdot L_k$ for $\mu > 1$ in order to guarantee $F(\mathbf{V}_{L_k}(\mathbf{x}^k)) \leq \mathcal{Q}_{L_k}(\mathbf{V}_{L_k}(\mathbf{x}^k); \mathbf{x}^k)$. In our experiments, we use $\mu := 2$.

A. *Joint values of parameters:* $\beta_q = \beta_t$ and $L_{cs} = L_\theta$

The results of our first test are presented in Table IV. In terms of number of iterations, we can observe that fixing L_k results in a poor performance and tends to increase the number of iterations as well as the final violation of the constraints. Given this poor performance, we do not consider the *Fixed* strategy for the remainder of the numerical experiments. Note that although Algorithm 1 achieves slow progress when fixing the parameters at the upper bounds, its convergence trend is still toward a stationary point, which confirms our theoretical results in the main text.

TABLE IV

PERFORMANCE RESULTS OF THE GAUSS-NEWTON ALGORITHM WITH DIFFERENT STRATEGIES FOR β AND L . THE THREE COLUMNS SHOW THE NUMBER OF ITERATIONS, AND THE MAXIMUM VIOLATION OF THE QUADRATIC (RESP. TRIGONOMETRIC) CONSTRAINT, RESPECTIVELY FOR EACH STRATEGY ON THREE PROBLEM INSTANCES.

Test Case	β	Fixed				Bisection				Geometric-2			
		# It	MVQ	MVT		# It	MVQ	MVT		# It	MVQ	MVT	
1354pegase	10	69	$9e^{-4}$	$2e^{-8}$	16	$3e^{-4}$	$1e^{-8}$	10	$3e^{-4}$	$7e^{-8}$			
	100	76	$4e^{-4}$	$1e^{-8}$	5	$2e^{-4}$	$2e^{-8}$	5	$1e^{-4}$	$6e^{-8}$			
	1,000	74	$3e^{-4}$	$1e^{-8}$	6	$7e^{-5}$	$6e^{-9}$	4	$1e^{-4}$	$4e^{-8}$			
1888rte	10	100	$1e^{-3}$	$4e^{-8}$	100	$8e^{-4}$	$4e^{-8}$	100	$8e^{-4}$	$4e^{-8}$			
	100	100	$1e^{-3}$	$4e^{-8}$	60	$1e^{-3}$	$6e^{-9}$	100	$7e^{-4}$	$4e^{-8}$			
	1,000	100	$1e^{-3}$	$2e^{-8}$	5	$9e^{-4}$	$3e^{-8}$	33	$8e^{-4}$	$3e^{-8}$			
1951rte	10	75	$9e^{-4}$	$7e^{-8}$	73	$9e^{-5}$	$3e^{-8}$	71	$9e^{-5}$	$3e^{-8}$			
	100	75	$9e^{-4}$	$7e^{-8}$	88	$4e^{-4}$	$3e^{-8}$	62	$7e^{-4}$	$2e^{-8}$			
	1,000	75	$9e^{-4}$	$7e^{-8}$	15	$8e^{-5}$	$7e^{-9}$	34	$5e^{-5}$	$3e^{-8}$			

Bisection and *Geometric-2* exhibit a similar behavior: they converge in tens of iterations, depending on the test case and the choice of β . Also, the tendency is for larger choices of β to require fewer iterations for convergence. To this end, we do not consider $\beta = 10$ in the remaining of the experiments. Nevertheless, the maximum violation of the quadratic constraint (MVQ) never reaches the desired tolerance of $1e^{-5}$. This behavior might suggest that we do not penalize sufficiently the quadratic constraint. This observation is confirmed by Fig. 2, which presents the evolution of the constraint violations for the 1354pegase test case, with $\beta = 10$ for the *Fixed* strategy. Nearly identical behavior has been observed in all the instances where the number of iterations exceeds 50. We observe that the maximum violation of the trigonometric constraint quickly reaches the target tolerance of $1e^{-5}$ (after around 5 iterations), while the maximum violation of the quadratic constraint exhibits very slow convergence.

One should notice that the quadratic and trigonometric constraints are linked: once the angles are fixed, c and s , which are the variables that appear in the quadratic constraints, struggle to move from their current value in order to satisfy the quadratic constraints. This motivates us to consider two different values for β and L_k : β_q for the quadratic constraints and L_{cs} for the associated variables c and s , and β_t for the trigonometric constraints, and L_θ for the additional variables they take into account, θ .

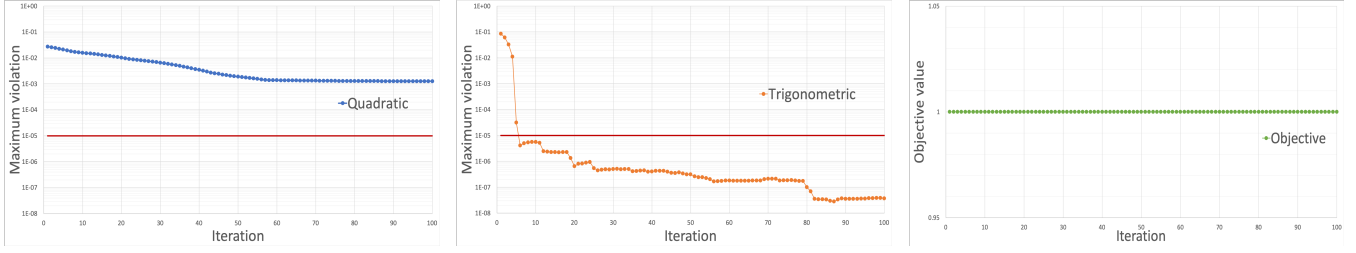


Fig. 2. The convergence behavior of the maximum violation of the quadratic and tangent constraints and the objective function values along w.r.t. the iterations for the case1888rte test case with $\beta = 100$ and a fixed value of L .

B. Individual choices of parameters: β_q , β_t and L_{cs} and L_θ

Based on our observation, we choose different values for β_q and β_t . Since we empirically observe that the quadratic constraints seem harder to satisfy than the trigonometric constraints, we consider two alternatives: $\beta_q = 2\beta_t$ and $\beta_q = 5\beta_t$. Note that the choice of different values for these parameters does not affect the theoretical guarantees of our algorithm as long as they satisfy our given conditions.

Also, since we have different values L_{cs} and L_θ , we must adapt the condition under which L_{cs} and L_θ are updated. From the theory, L is updated (through the *Bisection* or *Geometric* strategy) if the following condition is not met:

$$\begin{aligned}
 & F(\mathbf{x}^{k+1}) \leq \mathcal{Q}_L(\mathbf{x}^{k+1}; \mathbf{x}^k) \\
 \Leftrightarrow & \\
 & \beta_q \sum_{(i,j) \in \mathcal{L}} |\Psi_q^{ij}(\mathbf{c}^{k+1}, \mathbf{s}^{k+1})| \\
 & + \beta_t \sum_{(i,j) \in \mathcal{L}} |\Psi_t^{ij}(\mathbf{c}^{k+1}, \mathbf{s}^{k+1}, \boldsymbol{\theta}^{k+1})| \\
 \leq & \beta_q \phi_q(\mathbf{c}^k, \mathbf{s}^k, \mathbf{dc}^*, \mathbf{ds}^*) + \beta_t \phi_t(\mathbf{c}^k, \mathbf{s}^k, \boldsymbol{\theta}^k, \mathbf{dc}^*, \mathbf{ds}^*, \mathbf{d}\boldsymbol{\theta}^*) \\
 & + \frac{L_{cs}}{2} \|(\mathbf{dc}^*, \mathbf{ds}^*)\|^2 + \frac{L_\theta}{2} \|(\mathbf{d}\boldsymbol{\theta}^*)\|^2
 \end{aligned}$$

where $\mathbf{x}^{k+1} = \mathbf{x}^k + \mathbf{d}^*$.

We adapt this condition to the specific type of constraint. Concretely:

- If
$$\begin{aligned}
 & \beta_t \sum_{ij \in \mathcal{L}} |\Psi_t^{ij}(\mathbf{c}^{k+1}, \mathbf{s}^{k+1}, \boldsymbol{\theta}^{k+1})| \\
 & \leq \beta_t \Phi_t(\mathbf{c}^k, \mathbf{s}^k, \boldsymbol{\theta}^k, \mathbf{dc}^*, \mathbf{ds}^*, \mathbf{d}\boldsymbol{\theta}^*) \\
 & + \frac{L_{cs}^k}{2} \|(\mathbf{dc}^*, \mathbf{ds}^*)^\top\|^2 + \frac{L_\theta^k}{2} \|(\mathbf{d}\boldsymbol{\theta}^*)\|^2
 \end{aligned} \quad (37)$$

then update L_{cs}^k and L_θ^k .

- If (37) does not hold and

$$\begin{aligned}
 & \beta_q \sum_{ij \in \mathcal{L}} |\Psi_q^{ij}(\mathbf{c}^{k+1}, \mathbf{s}^{k+1})| \\
 & \leq \beta_q \Phi_q(\mathbf{c}^k, \mathbf{s}^k, \mathbf{dc}^*, \mathbf{ds}^*) + \frac{L_{cs}^k}{2} \|(\mathbf{dc}, \mathbf{ds})^\top\|^2
 \end{aligned} \quad (38)$$

then only update L_{cs}^k .

The results are presented in Table V. Overall, the number of iterations as well as the violations of the constraints at the end of the algorithm are decreasing compared to Table IV. This indicates that our parameter tuning strategy is promising for our algorithm. Concerning the values of β_t and β_q , it

seems that the larger they are, the better the performance that we achieve. For this reason, we drop $\beta_t = 100$ and consider also a value of β_t which depends on the data of the problems for the remaining simulations. We specifically set β_t equal to the number of lines, i.e. $\beta_t = |\mathcal{L}|$. The *Geometric-2* strategy appears to provide a better balance for the violation of the constraints even if it requires more iterations until convergence compared to the *Bisection* method (see 1888rte for the worst-case scenario). Nevertheless, we retain *Geometric-2* because it provides more promising results in terms of constraint violation (which is the most difficult criterion to achieve), and there is still room for improvement as we demonstrate in Appendix D. Finally, for the scale of β_q compared to β_t , even if $\times 5$ appears to be more promising, we still consider $\times 2$ in the simulations in order to observe the effect of the choice of β on the performance of our algorithm.

TABLE V
PERFORMANCE BEHAVIOR OF THE GAUSS-NEWTON ALGORITHM WITH DIFFERENT STRATEGIES FOR β_q , β_t , L_{cs} , L_θ .

Test Case	β_t	β_q	Bisection			Geometric-2		
			# It	MVQ	MVT	# It	MVQ	MVT
1354pegase	100	$\times 2$	5	$8e^{-5}$	$3e^{-8}$	4	$8e^{-5}$	$1e^{-8}$
	100	$\times 5$	4	$1e^{-4}$	$2e^{-8}$	4	$1e^{-4}$	$4e^{-8}$
	1,000	$\times 2$	5	$1e^{-4}$	$3e^{-10}$	4	$1e^{-4}$	$1e^{-8}$
	1,000	$\times 5$	5	$2e^{-5}$	$4e^{-10}$	3	$3e^{-6}$	$8e^{-6}$
1888rte	100	$\times 2$	13	$1e^{-3}$	$3e^{-8}$	100	$6e^{-4}$	$8e^{-8}$
	100	$\times 5$	8	$1e^{-3}$	$5e^{-8}$	100	$6e^{-4}$	$1e^{-7}$
	1,000	$\times 2$	5	$8e^{-4}$	$3e^{-8}$	100	$6e^{-4}$	$3e^{-8}$
	1,000	$\times 5$	5	$5e^{-4}$	$4e^{-8}$	15	$5e^{-4}$	$6e^{-9}$
1951rte	100	$\times 2$	63	$2e^{-4}$	$4e^{-8}$	50	$5e^{-5}$	$1e^{-8}$
	100	$\times 5$	32	$9e^{-5}$	$2e^{-8}$	76	$9e^{-6}$	$4e^{-6}$
	1,000	$\times 2$	10	$6e^{-5}$	$1e^{-8}$	39	$2e^{-5}$	$8e^{-8}$
	1,000	$\times 5$	8	$9e^{-6}$	$2e^{-8}$	3	$8e^{-6}$	$3e^{-6}$

APPENDIX D

AN IMPROVEMENT OF ALGORITHM 1 BY DECREASING THE NUMBER OF L UPDATES

We emphasize that, in Algorithm 1, each time that the values of L_t and/or L_q are updated, the subproblem \mathcal{P}_{sub}^k is resolved. Therefore, an effective strategy for updating these parameters can lead to significant improvements in computational time. We mitigate this heavy computational requirement by introducing resolution techniques that are guided by both our theoretical results and empirical observations.

Concretely, we propose the following two improvements to the practical implementation of the algorithm, in order to limit the number of computationally expensive L updates:

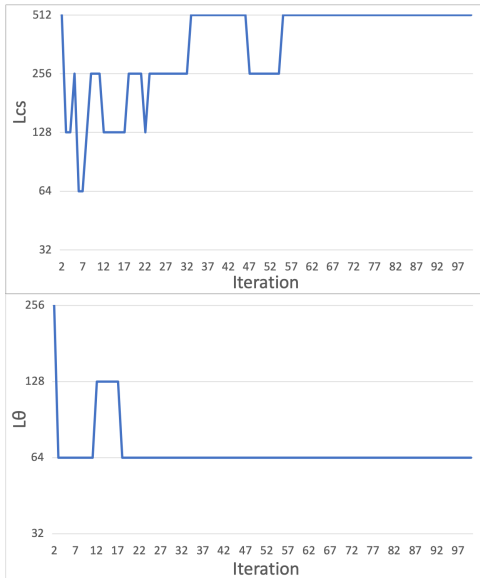


Fig. 3. The variation of L_{cs} and L_θ along the iterations for 1888rte when $\beta_t = 1,000$ and $\beta_q = 2,000$ (Geometric-2 strategy).

- 1) Using $L := \max(1, L/2)$ from one iteration to another is a better strategy than having $L := 1$ at the beginning of each iteration. We justify this on the basis of the observation of Fig. 3, which indicates that the appropriate value of L in a given iteration is a relatively accurate indicator of the appropriate value of L for the next iteration. Concretely, we observe that the value of L_θ does not change beyond iteration 18. On the other hand, the value of L_{cs} varies by only a factor of 4 until iteration 64, and stabilizes thereafter. This adaptation is essential to the efficient behavior of the algorithm. For example, we note that without this adaptation we require the resolution of 939 subproblems for solving instance 18888rte when using $\beta_t = 1,000$ and $\beta_q = 2,000$ with Geometric-2.
- 2) Checking conditions (37) and (38) can require a large number of L updates. Instead, we propose replacing these conditions with a verification of whether the violation of the constraints is decreasing, which is a less stringent requirement that still yields satisfactory results in terms of constraint violations. Concretely, at iteration k , we compute the ℓ_1 and ℓ_∞ norms of $\Psi_q(\mathbf{c}^k, \mathbf{s}^k)$ and $\Psi_t(\mathbf{c}^k, \mathbf{s}^k, \boldsymbol{\theta}^k)$. If these quantities decrease from $k-1$ to k , we move to iteration $k+1$.

By applying the new initial value of L_{cs} and L_θ at each iteration and by observing the decrease of the constraint violations $\Psi_q(\mathbf{c}^k, \mathbf{s}^k)$ and $\Psi_t(\mathbf{c}^k, \mathbf{s}^k, \boldsymbol{\theta}^k)$ in terms of the ℓ_1 -norm or ℓ_∞ -norm, we obtain the results that are presented in Table VI.

From Table VI, we observe that this new strategy leads to convergence for all three test cases. The choice of $\beta_t = |\mathcal{L}|$ seems promising and accelerates the algorithm by applying a less conservative criterion. For the test case 1888rte, which appears to be the most difficult one of the three test cases, our algorithm converges faster by solving a few tens of subproblems. We keep this setting for the comparison with

TABLE VI
PERFORMANCE RESULTS OF THE GAUSS-NEWTON ALGORITHM WITH DIFFERENT Geometric STRATEGY FOR $\beta_q = 2\beta_t$ AND $\beta_q = 5\beta_t$. HERE L IS HANDLED THROUGH L_{cs} AND L_θ WITH SPEED-UP. NOTE THAT WE REPORT THE NUMBER OF ITERATIONS (IT) AS WELL AS THE NUMBER OF TIMES THAT L_{cs} AND L_θ ARE UPDATED IN THE COLUMN '# IT + L'.

Test Case	β_t	$\beta_q = 2\beta_t$ and Geometric-2			$\beta_q = 5\beta_t$ and Geometric-2		
		# It + L	MVQ	MVT	# It + L	MVQ	MVT
1354pegase	1,000	4+0	$9e^{-6}$	$1e^{-6}$	4+0	$8e^{-6}$	$6e^{-7}$
	$ \mathcal{L} = 1,991$	4+0	$9e^{-6}$	$2e^{-6}$	4+0	$9e^{-6}$	$8e^{-7}$
1888rte	1,000	40+42	$6e^{-5}$	$3e^{-8}$	31+35	$4e^{-5}$	$5e^{-9}$
	$ \mathcal{L} = 2,531$	20+21	$6e^{-5}$	$1e^{-8}$	27+28	$9e^{-6}$	$6e^{-7}$
1951rte	1,000	3+0	$3e^{-6}$	$4e^{-6}$	3+0	$3e^{-7}$	$2e^{-7}$
	$ \mathcal{L} = 2,596$	3+0	$3e^{-7}$	$2e^{-7}$	3+0	$3e^{-7}$	$1e^{-7}$

IPOPT.

REFERENCES

- [1] A.M. Ostrowski. *Solutions of Equations and Systems of Equations*. Academic Press, New York, 1966.